DMD Fast Forward. Published on March 10, 2017 as DOI: 10.1124/dmd.116.074609
This article has not been copyedited and formatted. The final version may differ from this version.

In vitro interactions of epacadostat and its major metabolites with human efflux and uptake transporters: Implications for pharmacokinetics and drug interactions

Qiang Zhang, Yan Zhang, Jason Boer, Jack G. Shi, Peidi Hu, Sharon Diamond, and Swamy Yeleswaram

Incyte Corporation, Wilmington, DE 19803

Running title: **Interactions of Epacadostat with Transporters**

Corresponding Author:

Qiang Zhang, Ph.D.

Incyte Corporation

1801 Augustine Cut-Off

Wilmington, DE 19803

Email: qizhang@incyte.com

Phone: 302-498-5827

Fax: 302-425-2759

Number of Text Pages: 24

Number of Figures: 8

Number of Tables: 6

Number of References: 24

The number of words of Abstract: 247

The number of words of Introduction: 655

The number of words of Discussion: 1487

Non-standard Abbreviations:

EPAC, epacadostat; IDO1, indoleamine 2,3-dioxygenase 1; EHC, enterohepatic circulation; NME, new chemical entity; TEER, transepithelial electrical resistance; HBSS, Hank's Balanced Salt Solution; KO, knockout; CSA, cyclosporin A; IC_{50}, half-maximal inhibitory concentration; ER, efflux ratio

DMD Fast Forward. Published on March 10, 2017 as DOI: 10.1124/dmd.116.074609
This article has not been copyedited and formatted. The final version may differ from this version.

Abstract

Epacadostat (EPAC) is a first-in-class, orally active inhibitor of the enzyme indoleamine 2,3-dioxygenase 1 (IDO1) and has demonstrated promising clinical activity. In humans, three major plasma metabolites were identified: M9 (a glucuronide-conjugate), M11 (a gut microbiota metabolite), and M12 (a secondary metabolite formed from M11). It is proposed that the biliary excretion of M9, the most abundant metabolite, leads to the enterohepatic circulation of EPAC suggested by the human pharmacokinetics of EPAC. The in vitro interactions of EPAC and its major metabolites with major drug transporters involved in drug absorption and disposition were evaluated using various in vitro systems. EPAC is a substrate for efflux transporters, P-gp and BCRP, but not a substrate for hepatic uptake transporters, OATP1B1 and OATP1B3. The low permeability of M9 suggests an essential role for transporters in its disposition. M9 is likely excreted from hepatocytes into bile via MRP2 and BCRP, excreted into blood via MRP3, and transported from blood back into hepatocytes via OATP1B1 and OATP1B3. M11 and M12 are not substrates for P-gp, OATP1B1 or OATP1B3, and M11, but not M12, is a substrate for BCRP. With respect to inhibition of drug transporters, the potential of EPAC, M9, M11, and M12 to cause clinical DDIs via inhibition of P-gp, BCRP, OATP1B1, OATP1B3, OAT1, OAT3, or OCT2 was estimated to be low. The current investigation underlines the importance of metabolite-transporter interactions in the disposition of clinically relevant metabolites, which may have implications for the pharmacokinetics and drug interactions of parent drugs.

DMD Fast Forward. Published on March 10, 2017 as DOI: 10.1124/dmd.116.074609
This article has not been copyedited and formatted. The final version may differ from this version.

Introduction

Indoleamine 2,3-dioxygenase 1 (IDO1) is an enzyme that is upregulated in some tumor types and exerts immunosuppressive function by enhancing generation and activation of regulatory T cell and allowing tumors to escape immune surveillance. Epacadostat (EPAC) is an investigational drug which is a first-in-class, orally bioavailable small-molecule IDO1 inhibitor with high potency and selectivity. In clinical trials, patients with melanoma have been treated with EPAC in combination with ipilimumab, a cytotoxic T-lymphocyte-associated protein 4 (CTLA-4) inhibitor. EPAC is currently in several clinical trials in combination with immune checkpoint inhibitors, programmed cell death-1 (PD-1) and programmed cell death ligand-1 (PD-L1), in a variety of cancers.

Preclinical research has shown that the liver is the primary organ for the clearance of EPAC and its major metabolites with minimal renal clearance (unpublished results). Boer et al (Boer et al., 2016) have identified three major, IDO1-inactive, circulating EPAC metabolites in human plasma: M9, a direct O-glucuronide of EPAC formed by UGT1A9; M11, an amidine formed via gut microbiota from EPAC; and M12, an N-dealkylated metabolite of M11 formed via CYP enzymes (Fig. 1). In humans, M11 and M12 were detected at levels that were 30% and 80% of EPAC at steady state, respectively. In contrast, formation of M9, the EPAC glucuronide, is the dominant elimination pathway with an 8.0-fold greater $AUC_{0\text{-}12h}$ value than that of EPAC at steady state (Boer et al., 2016). Enterohepatic circulation (EHC) is a dispositional process of many drugs that undergo glucuronidation. This occurs by biliary excretion of the glucuronide conjugate and intestinal reabsorption of parent drug, often with hepatic conjugation and intestinal deconjugation (Dobrinska, 1989). Because M9 is the most abundant plasma metabolite of EPAC and double-peaks of EPAC were observed in the plasma concentration-time profiles of some human subjects (Fig. 2), involvement of EHC in the disposition of EPAC is likely. Furthermore, our previous study (Boer et al., 2016) revealed that when M9 was incubated with human feces homogenate, M9 was almost completely consumed in 24 hours with EPAC

DMD Fast Forward. Published on March 10, 2017 as DOI: 10.1124/dmd.116.074609
This article has not been copyedited and formatted. The final version may differ from this version.

and M11 being the two major products observed, suggesting the de-glucuronidation of M9 to form EPAC via gut microbiota. This finding supports the likely involvement of M9 in the EHC of EPAC.

It has been increasingly recognized by both regulatory agencies and pharmaceutical industry that drug transporters play important roles in absorption and disposition of a drug and therefore clinical drug-drug interactions (DDIs) (Giacomini et al., 2010). Numerous research articles investigating new chemical entity (NME)-transporter interactions have been published since the US Food and Drug Administration (FDA) and the European Medicines Agency (EMA) released the draft guidance on evaluation of drug interactions of investigational drugs (FDA, 2012; EMA, 2012) in 2012. However, the publications investigating metabolite-transporter interactions are still in their infancy. While metabolites are less likely to cause DDIs *via* inhibition of cytochrome P450 enzymes due to increased polarity and metabolic stability, reduced passive membrane permeability of metabolites makes them more susceptible to interactions with drug transporters (Zamek-Gliszczynski et al., 2014). In the present study, in order to gain a more complete understanding of the underlying mechanisms of the disposition and pharmacokinetics of EPAC, we adopted a comprehensive strategy to determine the in vitro interactions of both EPAC and its metabolites with the major drug transporters (P-pg, BCRP, OATP1B1, OATP1B3, OAT1, OAT3, and OCT2) and evaluate their potential as a perpetrator to cause transporter-mediated clinical DDIs employing a range of in vitro models. It has been demonstrated that MRP2 and MRP3 are critical efflux transporters in the disposition of many glucuronide conjugates in hepatocytes via biliary excretion and basolateral efflux of these conjugates, respectively (Zamek-Gliszczynski et al., 2006; de Waart et al., 2009; Köck and Brouwer, 2012; Zhang et al., 2016). Consequently, the EPAC glucuronide, M9, as the most abundant metabolite in human plasma, was further studied as a substrate for MRP2 and MRP3 to better understand the mechanisms of disposition of M9 in the liver and its implication for the pharmacokinetics of EPAC.

DMD Fast Forward. Published on March 10, 2017 as DOI: 10.1124/dmd.116.074609
This article has not been copyedited and formatted. The final version may differ from this version.

Materials and Methods

Materials

EPAC (free base) was synthesized by Adesis Inc. (New Castle, DE). M9 (INCB056867, free base) and M11 (INCB056868, free base) were generated by Hypha Discovery Ltd (Uxbridge, UK). M12 (INCB052101, free base) was synthesized by Incyte Corporation (Wilmington, DE). Dulbecco's modified Eagle medium (DMEM) and DMEM combined with Hams F12 (DMEM-F12) were purchased from Lonza (Basel, Switzerland). Fetal bovine serum (FBS), non-essential amino acids (NEAA), penicillin, streptomycin, and trypsin-EDTA were purchased from Mediatech (Manassas, VA). Estrone 3-sulfate, cerivastatin, cyclosporin A (CSA), benzbromarone, probenecid, metformin, verapamil, nadolol, metoprolol, prazosin, Ko143, quinidine, digoxin, sodium butyrate, and Hanks' balanced salt solution (HBSS) were purchased from Sigma-Aldrich (St Louis, MO). Pitavastatin calcium was purchased from Selleck Chemicals (Houston, TX). [^{3}H]Estrone 3-sulfate, [^{3}H]estradiol 17-β-glucuronide, [^{3}H]*p*-aminohippuric acid, and MicroScint-40 scintillation cocktail were purchased from PerkinElmer (Waltham, MA). [^{14}C]Metformin was purchased from Moravek (Brea, CA). BCA protein assay kit was purchased from Pierce Biotechnology (Rockford, IL). All other chemicals were of analytical grade and commercially available. The 24-well transwell plates with Polyethylene Terephthalate (PET) membrane filters, BioCoat™ collagen-coated 96-well plates, and BioCoat™ poly-L-lysine-coated 96-well plates were purchased from BD Bioscience (Bedford, MA).

Pharmacokinetic Evaluation of EPAC in Healthy Human Volunteers

A clinical Phase 1 study was conducted in healthy adult volunteers to evaluate the potential DDI between EPAC and warfarin, and the details of the study were described in a previous publication (Shi et al., 2016). Briefly, the study was comprised of 1 fixed sequence and 2 periods, enrolling 18 healthy adult volunteers. The subjects received a single dose of 25 mg warfarin (Coumadin® tablets) on Day 1 of Period 1 (Days 1-7) and again on Day 14 of Period 2 (Days 8-20). The subjects also received 300 mg EPAC two times a day during Days 8-20. Blood

DMD Fast Forward. Published on March 10, 2017 as DOI: 10.1124/dmd.116.074609
This article has not been copyedited and formatted. The final version may differ from this version.

samples for determination of plasma concentrations of EPAC and metabolites were collected at the following predetermined time points at pre-dose and 0.25, 0.5, 1, 1.5, 2, 3, 4, 6, 8, and 12 hours after administration of EPAC in the mornings on Days 13 and 14. The pharmacokinetic profiles of EPAC at steady state were determined using liquid chromatography-tandem mass spectrometry (LC-MS/MS).

Cell and Culture Conditions

Caco-2 cells were obtained from American Type Culture Collection (Rockville, MD). Madin-Darby canine kidney type II (MDCKII) cells, MDCKII cells stably transfected with human BCRP (MDCKII-BCRP), Chinese hamster ovary (CHO) cells, and CHO cells stably transfected with human OATP1B1 (CHO-hOATP1B1), OATP1B3 (CHO-hOATP1B3), OAT1(CHO-hOAT1), and OCT2 (CHO-hOCT2), human embryonic kidney 293 (HEK293) cells containing Flp-In™ system (Flp-In™-293) (Invitrogen) stably transfected with empty vector (Flp-In™-293-EV) and human OAT3 (Flp-In™-293-hOAT3) were obtained from Solvo Biotechnology (Budaörs, Hungary) under a license and service agreement.

All cells were grown at 37°C in an atmosphere of 5% CO_2. Both Caco-2 and MDCKII cells in DMEM growth medium supplemented with 10% (v/v) FBS, 1% (v/v) NEAA, penicillin (100 Unit/ml), and streptomycin (100 µg/ml). For MDCKII cells, 2 mM L-Glutamine was also added in the DMEM medium. Confluent cell monolayers were sub-cultured every seven days or four days for Caco-2 and MDCKII cells, respectively, by treatment with 0.25% trypsin containing 1 µM EDTA. Both Caco-2 and MDCKII cells were seeded in 24-well transwell plates. For bidirectional transport assays, Caco-2 cells and MDCKII cells were seeded at the density of 4,000 and 40,000 cells/well, respectively. Cell monolayers were used for transport assays between 22 and 25 days for Caco-2 cells and 4 days for MDCKII cells post-seeding. Both Flp-In™-293 and CHO cells were grown in DMEM-F12 growth medium supplemented with 10% (v/v) FBS, L-glutamine (2 mM), penicillin (100 Unit/ml), and streptomycin (100 µg/ml). For CHO cells, L-proline (50 µg/ml) was also added in the medium. Confluent cell monolayers were sub-cultured every two

DMD Fast Forward. Published on March 10, 2017 as DOI: 10.1124/dmd.116.074609
This article has not been copyedited and formatted. The final version may differ from this version.

or three days by treatment with 0.05% trypsin containing 1 μM EDTA. For uptake assays, CHO and Flp-In™-293 cells were seeded at a density of 4,000–10,000 cells/well in 96-well microplates coated with collagen I (CHO cells) or poly-L-lysine (Flp-In™-293 cells). Uptake experiments were carried out 24 to 48 hours post-seeding when cells were at least 90% confluent. For OATP1B1, OATP1B3, and OAT3 transfected cells, the cells were treated with 5 mM sodium butyrate for 24 hours before the experiment to increase the expression of transfected transporters (Gui et al., 2008).

Summary of In Vitro Models Used in the Present Article

For clarification of the choices of each in vitro model used to characterize the interactions of EPAC and its major metabolites with the drug transporters tested in this study, a summary table outlining the in vitro models, transporters, assay types, tested compounds, and primary purposes of using the individual models has been provided (see Table 1).

Transcellular Transport Assays in Caco-2 and MDCKII Cells

The transcellular transport studies in Caco-2 and MDCKII cells were carried out in house and the transcellular transport studies in transporter knock-out Caco-2 cells (MDR1/MRP2 and BCRP/MRP2 double-knockout) were conducted at BioReliance Corporation (Rockville, MD) under a service contract. All these studies were conducted by following similar procedures. Briefly, on the day of study, after cell culture medium was removed, cells were rinsed with HBSS (pH 7.4) and equilibrated for 10 min before the experiment. Transepithelial electrical resistance (TEER) was measured to ensure the integrity of the cell monolayers. For Caco-2 apparent permeability (P_{app}) assay, digoxin (5 μM, positive control P-gp substrate), EPAC, M9, M11, or M12 at 50 μM in HBSS was added to the donor chamber (apical side), while HBSS solution with 4% BSA was added in the receiver chamber (basolateral side). For bidirectional transport assays that were conducted in Caco-2 and MDCKII cells, digoxin, prazosin (positive control BCRP substrate), EPAC, M9, M11, or M12 at predetermined concentrations in HBSS buffer

DMD Fast Forward. Published on March 10, 2017 as DOI: 10.1124/dmd.116.074609
This article has not been copyedited and formatted. The final version may differ from this version.

without BSA were placed in either apical (A) or basolateral (B) side as donor chambers, while fresh HBSS buffer without BSA was placed in receiver chambers. The 24-well transwell plates were incubated at 37°C for 120 minutes. At the end of the incubation, 0.1 ml of sample was removed from the receiver and donor chambers, and an equal volume of acetonitrile was added to the sample for protein precipitation. The supernatant was collected after centrifugation for LC-MS/MS analysis.

Vesicular Uptake Studies using Membrane Vesicles Containing Human Efflux Transporters

The substrate studies of M9 for efflux transporters MRP2, MRP3, and BCRP were performed at BioReliance Corporation (Rockville, MD) under a service contract using inside-out membrane vesicles generated from the mammalian cells stably-expressing human BCRP, MRP2, or MRP3. Briefly, membrane suspensions were added to assay media on ice and dispensed into a 96-well plate (25 µg total membrane protein per well). Following a pre-incubation at 37ºC for 5 min, M9 (1–100 µM) was incubated for 8 min at 37ºC along with either 4 mM ATP or AMP (as negative control) in the presence or absence of positive control inhibitor of MRP2 (400 µM benzbromarone), MRP3 (1 mM sulfasalazine), or BCRP (1 µM Ko143). Positive control substrate of MRP2 (50 µM estradiol 17-β-glucuronide ($E_2$17βG)), MRP3 (50 µM $E_2$17βG) or BCRP (1 µM estrone 3-sulfate) and negative membrane control assays were carried out in the same plate. The reactions were stopped by adding ice-cold washing buffer. The reaction mixture was then transferred to a filter plate, and the liquid was removed under vacuum using a cell harvester. The filters were dried and subsequently analyzed by LC-MS/MS. Results were calculated as ATP-dependent transport and were expressed as pmol/min/mg protein. A rate of uptake for test compound ≥ 1.5–2 fold (relative to the AMP control) or 2 fold with inhibitor are considered a positive result.

Determination of EPAC and its Metabolites as Substrates of Human Hepatic Uptake Transporters

DMD Fast Forward. Published on March 10, 2017 as DOI: 10.1124/dmd.116.074609
This article has not been copyedited and formatted. The final version may differ from this version.

The potential for EPAC and its major metabolites to be a substrate of human hepatic uptake transporters OATP1B1 and OATP1B3 were determined using CHO cells stably transfected with OATP1B1 or OATP1B3. Pitavastatin was included as positive control substrate in the uptake experiments for both OATP1B1 and OATP1B3. These assays were conducted at 37°C using a 24-well format. After cell culture medium was removed, cells were washed once with pre-warmed Krebs-Henseleit **(**KH) buffer (142 mM NaCl, 23.8 mM $NaHCO_3$, 4.83 mM KCl, 0.96 mM K_2HPO_4, 12.5 mM HEPES, 1.53 mM $CaCl_2$, and 1.2 mM $MgSO_4$, pH 7.4). Uptake was initiated by adding 250 µl of KH buffer containing either the test compound (5 or 10 µM) or pitavastatin (0.5 µM). Cells were then incubated at 37°C for 1, 3, or 5 min (time-dependence studies). After the incubation, the uptake solution was rapidly aspirated and the cells were rinsed twice with 500 µl of ice-cold phosphate buffered saline (PBS) to stop uptake process. EPAC, M9, M11, M12, or pitavastatin that was accumulated in the cells was extracted by adding 250 µl of lysis solution (70:30 methanol:water (v:v)) to each well. Following shaking the plate for 30 min, the cells were scraped briefly to maximize recovery of the samples. Cell lysate was centrifuged for 10 min at 13,000 rpm at 4°C. The supernatant was transferred to a 96-well plate for analysis using LC-MS. Protein amount was quantified using BCA protein assay kit (Pierce Biotechnology) and the plate for protein quantification was read on an Enspire Multilabel Reader (PerkinElmer, Waltham, MA).

Determination of EPAC and its Metabolites as Inhibitors of Human Uptake Transporters

The potential for EPAC and its major metabolites to inhibit the transport of probe substrates for human uptake transporters OATP1B1, OATP1B3, OAT1, OAT3, and OCT2 were determined using CHO or Flp-In™-293 cells stably transfected with each correspondent transporter. EPAC, M9, M11, or M12 was dissolved in DMSO with final concentrations between 0.13 and 300 µM. Positive control inhibitors were 100 µM cerivastatin (OATP1B1), 10 µM cyclosporin A (OATP1B3), 200 µM benzbromarone (OAT1), 100 µM probenecid (OAT3), and 100 µM verapamil (OCT2). These assays were conducted at 37°C using a 96-well format with

DMD Fast Forward. Published on March 10, 2017 as DOI: 10.1124/dmd.116.074609
This article has not been copyedited and formatted. The final version may differ from this version.

substrates at the concentrations well below their respective K_m values. The probe substrates used in these studies included [^{3}H]estrone 3-sulfate (0.1 μM), [^{3}H]estradiol 17-β-glucuronide (0.2 μM), [^{3}H]*p*-aminohippuric acid (1 μM), [^{3}H]estrone 3-sulfate (0.24 μM), or [^{14}C]metformin (10 μM) for OATP1B1, OATP1B3, OAT1, OAT3, and OCT2, respectively. After cell culture medium was removed, cells were washed once with pre-warmed KH buffer. Uptake was initiated by adding 50 μl of KH buffer containing the probe substrate, EPAC, M9, M11, or M12 either in the presence or absence of a positive control inhibitor for each correspondent transporter. Cells were then incubated at 37°C for designated time. After the incubation, the uptake solution was rapidly aspirated and the cells were rinsed twice with 100 μl of ice-cold PBS to stop uptake process. Cells were solubilized by adding 50 μl of 0.2 N NaOH and incubating for 15 min at 37ºC. Cell lysate was transferred to a white solid-bottom 96-well plate, and then 150 μl of MicroScint-40 scintillation cocktail was added to each well. After 3 hours incubation in the dark at room temperature, radioactivity was determined by using a MicroBeta™ Microplate Scintillation Counter (PerkinElmer, Waltham, MA).

LC-MS/MS Analysis

Samples containing EPAC, M11, M12, digoxin, nadolol, metoprolol, prazosin or pitavastatin from transcellular transport and uptake experiments were analyzed by using a Shimadzu LCMS-2020 (Shimadzu Scientific Instruments, Columbia, MD) with a Zorbax SB-C18 column (2.1 x 50 mm, 3.5 μm; Phenomenex Inc., Torrance, CA). The chromatographic separation was achieved using a gradient elution consisting of mobile phase A (0.1% formic acid in water) and mobile phase B (0.1% formic acid in acetonitrile) at a flow rate of 500 μl/min. M9 samples were analyzed by turbo ion spray LC-MS/MS under gradient conditions. Chromatography was performed with an ACE 3 C8 HPLC column (2.1 × 50 mm, 3 μm; Advanced Chromatography Technologies, Aberdeen, Scotland) at ambient temperature with a gradient composed of mobile phase A (0.1% formic acid in water) and mobile phase B (0.1% formic acid in acetonitrile) at a flow rate of 300 μl/min. Peak areas were detected on a Sciex API-4000 (AB Sciex LLC, Foster

DMD Fast Forward. Published on March 10, 2017 as DOI: 10.1124/dmd.116.074609
This article has not been copyedited and formatted. The final version may differ from this version.

City, CA) operating in positive ionization mode with MRM transitions: m/z 614.2 → 438.0. Chromatographic peaks were integrated and quantitative analysis was performed using Analyst software (version 1.4.1).

Data Analysis

Apparent permeability coefficient (P_{app}) values from transcellular transport studies were determined using the following equation:

$$P_{app}\ (\text{cm/sec}) = (F * VD)/(SA * MD)$$

where the flux rate (F, mass/time) is calculated from the slope of cumulative amounts of compound of interest on the receiver side, SA is the surface area of the cell membrane, VD is the donor volume and MD is the initial amount of the solution in the donor chamber. The efflux ratio (ER) from Caco-2 and MDCKII studies was calculated as the ratio of the P_{app} measured in the B-A direction divided by the P_{app} in the A-B direction. BCRP-mediated net efflux was determined by dividing the ER obtained from MDCKII-BCRP cells by the ER from MDCKII-control cells.

The IC_{50} values for inhibition of digoxin and prazosin transport by test compound from Caco-2 and MDCKII studies were determined by fitting the curve onto the net efflux ratio versus concentrations of test compound using a dose-response method from Prism 6.02 (2007, GraphPad, San Diego, CA). The IC_{50} value for uptake transporters was defined as the concentration of inhibitor needed to inhibit transport of the probe substrate by 50% and was determined using Prism 6.02. The degree of inhibition of OATP1B1 or OATP1B3 in humans was estimated by a static model using the R value (Hirano et al., 2006; Giacomini et al., 2010), which represents the ratio of the uptake clearance in the absence of inhibitor to that in the presence of inhibitor:

$$R = 1 + (fu \times I_{in,max}/IC_{50})$$

$$I_{in,max} = C_{max} + (k_a \times Dose \times F_aF_g/Q_h)$$

DMD Fast Forward. Published on March 10, 2017 as DOI: 10.1124/dmd.116.074609
This article has not been copyedited and formatted. The final version may differ from this version.

where $I_{in,max}$ is the estimated maximum inhibitor concentration at the inlet to the liver, C_{max} is the maximum systemic plasma concentration of inhibitor, Dose is the inhibitor dose, F_aF_g is the fraction of the dose of inhibitor which is absorbed, k_a is the absorption rate constant of the inhibitor, and Q_h is the hepatic blood flow rate in humans (1500 ml/min). Statistical analysis was conducted using a Student *t* test for comparing two treatments. A *P* value < 0.05 was considered significant.

DMD Fast Forward. Published on March 10, 2017 as DOI: 10.1124/dmd.116.074609
This article has not been copyedited and formatted. The final version may differ from this version.

Results

Physicochemical Properties of EPAC and Its Metabolites

The absorption, distribution, metabolism, and excretion (ADME) of drugs and metabolites are profoundly influenced by their physicochemical properties such as molecular size, lipophilicity, polarity, and membrane permeability. The molecular weight, LogP, polar surface area (PSA), and apparent permeability values for EPAC, M9, M11, and M12 were summarized in Table 2. While the Caco-2 permeability values were moderate for EPAC, M11, and M12 ranging from 3.2 to 9.3 x 10^{-6} cm/s, the value of M9 was very low (< 0.1 x 10^{-6} cm/s) (Table 2). This is expected because M9 as a direct glucuronide conjugate is more hydrophilic and polar with a low LogP value (-2.1) and a high PSA value (264).

Pharmacokinetic Profiles of EPAC in Human Subjects Suggesting EHC

After multiple twice daily oral dosing of 300 mg EPAC, the steady state plasma concentration-time profiles of EPAC in 5 subjects (5 out of 17 subjects; 29%) exhibited distinct secondary peaks at approximately 4 h postdose (Fig. 2), suggesting EHC of EPAC.

Evaluation of EPAC and Its Metabolites as P-gp and BCRP Substrates

Evaluation of EPAC and its metabolites as substrates of P-gp and BCRP was conducted in Caco-2 cell and BCRP-transfected MDCKII cell monolayers, respectively. Bi-directional transport experiments in Caco-2 cells indicated that the B-A/A-B efflux ratio (ER) of digoxin was 25. This ratio decreased to unity with the addition of the P-gp inhibitor CSA, indicating that P-gp expressed in the Caco-2 cells were functionally active. In the presence of CSA, the ER of EPAC was partially reduced (< 50%) (Fig. 3A), suggesting that P-gp contributes to the efflux of EPAC and other transporters may also play a role in the efflux of EPAC in Caco-2 cell monolayers. The ER of M9 was 2.5 and 1.9 at 1 or 20 μM, respectively, suggesting that the efflux of M9 in Caco-2 cells is minimal and it is unlikely a P-gp substrate (Fig. 3B). The ER values of M11 and

DMD Fast Forward. Published on March 10, 2017 as DOI: 10.1124/dmd.116.074609
This article has not been copyedited and formatted. The final version may differ from this version.

M12 at each concentration were below 2 (Fig. 3, C and D), indicating that neither M11 nor M12 is a substrate of P-gp.

The ratio of ER of EPAC in BCRP-MDCKII cells to that in control-MDCKII cells ($ER_{BCRP}/ER_{control}$) was 35 and 27 at 3 and 300 μM, respectively, indicating that EPAC is a substrate of BCRP and the efflux mediated by BCRP was not saturated at 300 μM (Fig. 3E). The $ER_{BCRP}/ER_{control}$ values of M11 were 93 and 48 at 10 and 300 μM, respectively, which suggests that M11 is a substrate of BCRP and its efflux mediated by BCRP was not saturated at 300 μM (Fig. 3G). The $ER_{BCRP}/ER_{control}$ values of M12 (1–300 μM) were around unity, indicating that M12 is not a substrate of BCRP (Fig. 3H). Because the permeability of M9 is very low and the bidirectional transport assay may underestimate the efflux ratios of low-permeability compounds (Brouwer et al., 2013), a vesicular uptake assay using membrane vesicles containing BCRP was carried out to determine whether M9 is a substrate of BCRP. The uptake rates of M9 into BCRP-expressing membrane vesicles in the presence of ATP, AMP, or combination of ATP and Ko143 were 115, 60.2, and 53.5 pmol/min/mg protein, respectively (Fig. 3F). This result implies that M9 is a substrate of BCRP.

To further evaluate the relative contribution of P-gp and BCRP in the efflux of EPAC in Caco-2 cells, an additional study was conducted in MDR1/MRP2 double KO and BCRP/MRP2 double KO Caco-2 cell lines. It has been demonstrated that these KO cell lines derived from Caco-2 cells (C2BBe1 clone) are similar to the wild type Caco-2 cells with respect to growth rate, morphology, differentiation, tight junction formation, passive permeability of model compounds, and stability of phenotype (Sampson et al., 2015). Two control substrates, digoxin (P-gp substrate) and estrone sulfate (BCRP substrate), were used in this study to ensure the validity of these KO models. As expected, verapamil (positive control inhibitor of P-gp) completely inhibited the efflux of digoxin in parental cells and BCRP/MRP2 KO cells, and Ko143 (positive control inhibitor of BCRP) reduced the efflux of estrone sulfate by 87% in parental cells and

DMD Fast Forward. Published on March 10, 2017 as DOI: 10.1124/dmd.116.074609
This article has not been copyedited and formatted. The final version may differ from this version.

100% in P-gp/MRP2 KO cells. In addition, the ER of digoxin was not reduced by double KO of BCRP and MRP2 (Fig. 4D) and the ER of estrone sulfate was not reduced by double KO of P-gp and MRP2 (Fig. 4B), confirming the function of P-gp and BCRP proteins in these KO cell lines and the specificity of KO of the individual efflux transporters. As shown in Figure 4, EPAC exhibited much higher efflux in the parental (ER = 24) and the P-gp/MRP2 KO cell lines (ER = 18) than BCRP/MRP2 KO cell line (ER = 4.2), indicating that BCRP may play a more important role in the efflux of EPAC in Caco-2 cells than P-gp. Verapamil partially inhibited efflux of EPAC in the parental cells (ER reduced from 15 to 10, 33% inhibition), and completely inhibited efflux in BCRP/MRP2 KO cells (ER reduced from 4.2 to 1.4) (Fig. 4C). The efflux of EPAC was inhibited by Ko143 (ER reduced from 24 to 5.5, 77% inhibition) in the parental cells to a greater extent than verapamil, and completely inhibited by Ko143 in the P-gp/MRP2 KO cells (ER reduced from 18 to 1.1) (Fig. 4A). These results suggest that EPAC is a substrate of both P-gp and BCRP, although it appears that BCRP may have more pronounced effect on the efflux of EPAC in Caco-2 cells.

Evaluation of EPAC and Its Metabolites as OATP1B1 and OATP1B3 Substrates

Given the important roles of OATP1B1 and OATP1B3 in the hepatic uptake of drugs and metabolites in humans, in vitro uptake studies were performed to investigate whether EPAC and its metabolites are substrates of these two uptake transporters by using CHO cells transfected with human OATP1B1 or OATP1B3. The uptake of EPAC into OATP1B1- or OATP1B3-transfected cells was approximately 1.8-fold or 2.2-fold greater than that in control cells, respectively (Fig. 5, A and E), suggesting that EPAC appears to be a poor substrate of both OATP1B1 and OATP1B3. The uptake of M9 into OATP1B1- or OATP1B3-transfected cells was at least 2.2-fold or 3.7-fold greater than those in control cells, respectively (Fig. 5, B and F), suggesting that M9 is likely a substrate of these two transporters. In contrast, because the uptake of M11 and M12 into OATP1B1- or OATP1B3-transfected cells was less than 2-fold (1.2

DMD Fast Forward. Published on March 10, 2017 as DOI: 10.1124/dmd.116.074609
This article has not been copyedited and formatted. The final version may differ from this version.

to 1.7-fold) of that in control cells (Fig. 5, C, D, G and H), it is unlikely that M11 and M12 are substrates of OATP1B1 and OATP1B3.

As per the decision tree in the FDA guidance (FDA, 2012), additional experiments were performed using cerivastatin as a positive control inhibitor of OATP1B1 and OATP1B3 to confirm whether EPAC and M9 are substrates of OATP1B1 and OATP1B3. Pitavastatin was used as a positive control substrate in these experiments. The uptake of pitavastatin into OATP1B1- or OATP1B3-transfected cells was significantly reduced by cerivastatin, indicating the effectiveness of the inhibitor treatment (Fig. 6, C, D, G, and H). The uptake of EPAC into OATP1B1- or OATP1B3 transfected cells in the presence of cerivastatin was not significantly different from that of the vehicle control, implying that EPAC is not a substrate of OATP1B1 or OATP1B3 (Fig. 6, A and B). In contrast to EPAC, cerivastatin reduced the uptake of M9 into OATP1B1- and OATP1B3-transfected cells by 91% and 81%, respectively (Fig. 6, E and F). These results confirm that M9 is a substrate of both OATP1B1 and OATP1B3.

Evaluation of M9 as a Substrate for MRP2 and MRP3

Because M9 is a glucuronide conjugate of EPAC with low membrane permeability and exhibited high systemic exposure (up to 8-fold of EPAC exposure) in humans, MRP2 and MRP3 are likely involved in the hepatic disposition of this glucuronide metabolite. The interactions of M9 with MRP2 and MRP3 as a substrate were determined using the membrane vesicles harvested from human MRP2 or MRP3-transfected cells. M9 was taken up and accumulated to a greater extent (4.7-fold higher) in the MRP2-containing vesicles compared to the negative control membrane vesicles. The accumulation of M9 in the MRP2-containing vesicles was inhibited by AMP and benzbromarone (positive control inhibitor) by 78 and 89%, respectively (Fig. 7A). The accumulation of M9 in the MRP3-containing vesicles was 24-fold greater than that in the negative control membrane vesicles. Both AMP and sulfasalazine (positive control inhibitor)

DMD Fast Forward. Published on March 10, 2017 as DOI: 10.1124/dmd.116.074609
This article has not been copyedited and formatted. The final version may differ from this version.

strongly inhibited the accumulation of M9 in the MRP3-containing vesicles (> 90% inhibition) (Fig. 7B). These results clearly indicate that M9 is a substrate for MRP2 and MRP3.

Evaluation of EPAC and Its Metabolites as P-gp and BCRP Inhibitors

To determine whether P-gp is inhibited by EPAC and its metabolites, the ER of digoxin in Caco-2 cells was examined in the absence or the presence of various concentrations of EPAC, M9, M11 or M12. The ER of digoxin decreased in the presence of EPAC in a concentration-dependent manner. At 500 μM EPAC, the ER of digoxin reduced by only 45%, suggesting that the IC_{50} of EPAC is greater than 500 μM (Table 3). No significant decrease in the ER of digoxin was observed in the presence of M9, M11, or M12 over the concentrations between 0 and 300 μM, therefore these metabolites are not inhibitors of P-gp (Table 3).

The potential of EPAC and its metabolites to inhibit BCRP was determined in MDCKII-BCRP cell line. Prazosin was used as a prototype substrate of BCRP (Ni et al., 2010), and Ko143 was used as a BCRP inhibitor (Allen et al., 2002). The $ER_{BCRP}/ER_{control}$ value of prazosin was not reduced in the presence of various concentrations of EPAC or M9 (0–300 μM), which indicates that EPAC and M9 are not inhibitors of BCRP. The BCRP-mediated efflux of prazosin was slightly reduced in the presence of various concentrations of M11 (0–300 μM), and the IC_{50} value was greater than 300 μM. M12 inhibited the BCRP-mediated efflux of prazosin significantly with an IC_{50} value of 32 μM (Table 3). Overall, the potential of both EPAC and its metabolites to cause clinical DDIs via inhibition of P-gp or BCRP is low because the ratios of I_1/IC_{50} are below 0.1 and the ratios of I_2/IC_{50} are below 10 based on the FDA guidance on DDI evaluation (Table 4).

Evaluation of EPAC and Its Metabolites as Inhibitors of OATP1B1, OATP1B3, OAT1, OAT3 and OCT2

DMD Fast Forward. Published on March 10, 2017 as DOI: 10.1124/dmd.116.074609
This article has not been copyedited and formatted. The final version may differ from this version.

The potential of EPAC and its metabolites to inhibit the human hepatic uptake transporters OATP1B1 and OATP1B3, and the human renal uptake transporters OAT1, OAT3, and OCT2 was determined in individual transporter-expressing CHO or HEK293 cell lines. EPAC was not a potent inhibitor of OCT2 with an IC_{50} value > 100 µM, but inhibited the uptake mediated by OAT3, OATP1B3, and OATP1B1 with the IC_{50} values of 21, 51, and 59 µM, respectively. M9 was a weak inhibitor of OAT3 and OATP1B1 with the IC_{50} values > 200 µM, and inhibited the uptake mediated by OATP1B3 with an IC_{50} of 27 µM. M11 inhibited the uptake mediated by OAT3, OATP1B3, OCT2, and OATP1B1 with the IC_{50} values of 14, 19, 23 and 68 µM, respectively. M12 was a weak inhibitor of OATP1B3 with an IC_{50} value > 200 µM, and inhibited the uptake mediated by OAT1, OAT3, OCT2, and OATP1B1 with the IC_{50} values of 8.6, 21, 21 and 49 µM, respectively (Table 3).

The calculated ratios of total C_{max}/IC_{50} for hepatic uptake transporters OATP1B1 and OATP1B3 and the ratios of unbound C_{max}/IC_{50} for renal uptake transporters OAT1, OAT3, and OCT2 are less than 0.1 except that the ratios of total C_{max}/IC_{50} of M9 and M11 for OATP1B3 are greater than 0.1 (0.38 and 0.11, respectively) (Tables 5 and 6). Because the ratios of total C_{max}/IC_{50} of M9 and M11 for OATP1B3 are greater than 0.1, the R values of M9 and M11 were calculated using extrapolation (Table 5) by following the decision tree in the FDA guidance (FDA, 2012). The estimation of $I_{in,max}$ of metabolites is difficult because parameters such as k_a, F_a, F_g and dose are difficult to estimate. For this reason, the R values of M9 and M11 were calculated using total C_{max} instead of $I_{in,max}$, therefore the R values may be underestimated. Because $F_a x F_g$ and ka are not known, $F_a x F_g$ and ka values were set as 1 and 0.1, respectively, the resulting R values are less than the cut-off value of 1.25 by FDA, suggesting a low potential of the two metabolites to cause OATP1B3-mediated DDI. In general, the potential of EPAC and its metabolites to cause clinical DDIs via inhibition of OATP1B1, OATP1B3, OAT1, OAT3, or OCT2 is low based on their exposure and inhibitory potency.

DMD Fast Forward. Published on March 10, 2017 as DOI: 10.1124/dmd.116.074609
This article has not been copyedited and formatted. The final version may differ from this version.

Discussion

In the current investigation, we took a comprehensive approach to determine the in vitro interactions of both EPAC and its major metabolites with key drug transporters involved in drug absorption and disposition, and assessed their potential to cause transporter-mediated DDIs. By following this approach, we were able to understand the molecular mechanisms of the disposition of both EPAC and its metabolites in humans and elucidate the complex process of metabolism, transport, and enzyme-transporter interplay. With such important information, our understanding of the underlying mechanisms of the pharmacokinetics of EPAC can be substantially improved and the ongoing clinical development of this promising investigational drug can benefit from the knowledge derived from this investigation.

EPAC is found to be a substrate of P-gp and BCRP, which are key efflux transporters expressed in human intestine, brain, liver, and kidney. In a clinical pharmacokinetic study, the exposure of EPAC increased in a dose-proportional manner in the range of 50-400 mg BID. Therefore, the role of efflux transporters, including P-gp and BCRP, in limiting oral absorption of EPAC might be insignificant at the doses (up to 300 mg BID) used in the clinical development. While the uptake of EPAC was higher in CHO cells expressing OATP1B1 or OATP1B3 than that in control cells, the uptake of EPAC was not significantly inhibited by an inhibitor of OATP1B, cerivastatin. Therefore, EPAC may not be a substrate for OATP1B1 or OATP1B3. Given its moderate membrane permeability, the major route for EPAC to enter hepatocytes may be through passive diffusion.

The involvement of EHC in the disposition of EPAC is suggested by the distinct secondary peaks in the profiles of EPAC in healthy human subjects (Fig. 2). We postulated that the glucuronide conjugate M9 (the most abundant circulating metabolite) may participate in the EHC of EPAC because glucuronide metabolites are frequently shown to be involved in EHC of a drug. Thus, the interactions of M9 with hepatic drug transporters were investigated to gain insight of

DMD Fast Forward. Published on March 10, 2017 as DOI: 10.1124/dmd.116.074609
This article has not been copyedited and formatted. The final version may differ from this version.

the disposition of M9 in the liver and its implication for the pharmacokinetics of EPAC. While EPAC, M11, and M12 exhibit moderate permeability, the more hydrophilic M9 displays very low permeability in Caco-2 cells (Table 2), making it heavily reliant on interactions with transporters to cross cell membranes (Zamek-Gliszczynski et al., 2014). Among the major canalicular efflux transporters (MRP2, BCRP, and P-gp) responsible for biliary excretion of drugs and metabolites, MRP2 (Fig. 7A) and BCRP (Fig. 3F) likely participate in the biliary excretion of M9. Given its low permeability and high systemic exposure, we suspected that M9 may be excreted to blood by the basolateral efflux transporter MRP3 following its formation in hepatocytes. Our results indeed confirmed that M9 is a MRP3 substrate (Fig. 7B). Whether M9 is also a substrate of other basolateral efflux transporters (such as MRP4) remains to be determined. M9 is also shown to be taken up by OATP1B1 and OATP1B3, the major uptake transporters in the basolateral membrane of hepatocytes (Fig. 5, B and F), suggesting that the circulating M9 in the blood relies on uptake transporters to enter hepatocytes for its biliary excretion.

As illustrated in Figure 8, our data suggest that once formed within the hepatocytes by UGT1A9 enzyme, M9 relies on interactions with the canalicular efflux transporters MRP2 and BCRP to be excreted into the bile, the basolateral efflux transporter MRP3 to be excreted into the blood, and the basolateral uptake transporters OATP1B1 and OATP1B3 to be transported from the blood back into the hepatocytes for its subsequent biliary excretion. By preventing saturation of the canalicular efflux transporters in the upstream hepatocytes, these basolateral transporters (MRP3 and OATPs) present in the upstream and downstream hepatocytes may work in concert for efficient sinusoidal excretion and basolateral reuptake of M9. Similar to the interactions of M9 with the transporters in the liver, glucuronide conjugates of some drugs, including ezetimibe (Oswald et al, 2008; de Waart et al, 2009) and diclofenac (Zhang et al, 2016), are also excreted to blood by MRP3 and taken up by OATPs for their subsequent biliary excretion by canalicular efflux transporters (including MRP2 and BCRP). The recently reported phenomenon, “hepatocyte hopping”, is believed to be important in hepatic disposition of glucuronide

DMD Fast Forward. Published on March 10, 2017 as DOI: 10.1124/dmd.116.074609
This article has not been copyedited and formatted. The final version may differ from this version.

conjugates, such as bilirubin glucuronide (Iusuf et al., 2012) and sorafenib glucuronide (Vasilyeva et al., 2015). Vasilyeva *et al* hypothesized (Vasilyeva et al., 2015) that considering the broad substrate specificity of these hepatic transporters (MRPs and OATPs), other xenobiotics undergoing hepatic glucuronidation can be subject to the hepatocyte hopping process similar to that of sorafenib glucuronide. Although more studies are needed in this emerging area in the future, the transporter-mediated disposition of glucuronide metabolites of EPAC, ezetimibe, and diclofenac in the liver might support this hypothesis.

Potentially, modulation of the interactions of M9 with the transporters responsible for its disposition may have an impact on the pharmacokinetics of EPAC because of the high systemic exposure and possible involvement of M9 in the EHC of EPAC. In this regard, the observed clinical DDI between mycophenolate mofetil (an immunosuppressive drug) and cyclosporine (Pou et al, 2001; Shipkova et al, 2001; Zamek-Gliszczynski et al., 2014) and the impact of OATP1B3 polymorphism on the pharmacokinetics of mycophenolate mofetil (Picard et al, 2010; Zamek-Gliszczynski et al., 2014) may be a good example to demonstrate the importance of glucuronide metabolite-transporter interactions in the pharmacokinetics of a drug undergoing EHC. Mycophenolic acid (MPA) is the active metabolite of mycophenolate mofetil (a prodrug) and mycophenolic acid glucuronide (MPAG) contributes to the EHC of MPA. Coadministered cyclosporine may disrupt the EHC process of MPA by inhibiting the OATP1B-mediated uptake of MPAG. This led to elevated systemic concentrations of MPAG, reduced availability of MPA for EHC, and eventually a decrease in the systemic exposure of MPA (Picard et al, 2010). Similarly, the MPA exposure in the patients carrying a genetic variant of OATP1B3 was lower than that in the patients carrying wildtype OATP1B3 because the hepatic uptake of MPAG was impaired due to the reduced function of the OATP1B3 variant, and thus the biliary excretion of MPAG was decreased, resulting in the decreased EHC of MPA (Picard et al, 2010).

DMD Fast Forward. Published on March 10, 2017 as DOI: 10.1124/dmd.116.074609
This article has not been copyedited and formatted. The final version may differ from this version.

The potential of EPAC and its major metabolites to cause transporter-mediated clinical DDIs was also evaluated in the present study. Based on their inhibitory potency and human exposures, the risk of EPAC, M9, M11 and M12 to cause clinical DDIs *via* inhibition of Pgp, BCRP, OATP1B1, OATP1B3, OAT1, OAT3, or OCT2 was estimated to be low (Tables 4–6). It is worth noting that some challenges exist in evaluating the risk of transporter-mediated DDI caused by metabolites. One of these challenges is estimation of I_2 concentration (theoretical maximum concentration in the intestine). Usually, metabolite concentrations at the intestinal level are not readily calculable because the liver is the major site for metabolism. In the case of EPAC metabolism, M11 is formed from EPAC by the gut flora and majority of M9 is moved from the bile to the intestine where M9 can be de-conjugated to form EPAC. Consequently, it is difficult to determine the maximum intestinal concentrations of M11 and M9. Under the most conservative consideration, if all EPAC molecules following oral dose of 300 mg (the highest dose in the clinical development) are converted to M11 (in the intestine) or M9 (in the liver) with all M9 molecules moving to the intestine, the I_2 concentrations of M11 and M9 would be the same as that of EPAC (2740 μM). Thus, the ratios of I_2/IC_{50} of both metabolites would be less than 10, indicating low risk of DDIs due to inhibition of P-pg or BCRP. When the R value method is used to evaluate OATP1B-mediated DDIs, estimation of $I_{in,max}$ of metabolites is another challenge because some parameters, such as k_a, F_a, F_g and dose, of metabolites are difficult to estimate. In the cases of M9 and M11, the R values were calculated based on total C_{max} instead of $I_{in,max}$, therefore the R values may be underestimated.

In conclusion, the in vitro interactions of both EPAC and its major metabolites with key drug transporters involved in drug absorption and disposition were evaluated in this study. EPAC is shown to be a substrate for BCRP and P-gp, but not a substrate for OATP1B1 or OATP1B3. Given the likely involvement of M9 in the EHC of EPAC observed in humans, we also identified the transporters involved in the disposition of M9 (EPAC glucuronide) in the liver. M9 is a substrate for multiple uptake (OATP1B1 and OATP1B3) and efflux (MRP2, MRP3, and BCRP)

DMD Fast Forward. Published on March 10, 2017 as DOI: 10.1124/dmd.116.074609
This article has not been copyedited and formatted. The final version may differ from this version.

transporters. The pharmacokinetics of EPAC may be potentially influenced by modulation of the transporter-mediated disposition of M9 in the liver. The risk of EPAC and its major metabolites to cause clinical DDIs by inhibiting the drug transporters tested was estimated to be low. Our research underlines the importance of metabolite-transporter interactions in the disposition of clinically relevant metabolites, which may have implications for the pharmacokinetics and drug interactions of parent drugs.

Authorship Contributions

Participated in research design: Q. Zhang, Y. Zhang, Boer, Hu, Diamond, and Yeleswaram.

Conducted experiments: Q. Zhang, Y. Zhang, Boer, and Hu.

Performed data analysis: Q. Zhang, Y. Zhang, Boer, Shi, and Hu.

Wrote or contributed to the writing of the manuscript: Q. Zhang, Y. Zhang, Shi, Diamond, and Yeleswaram,

References

Allen JD, van Loevezijn A, Lakhai JM, van der Valk M, van Tellingen O, Reid G, Schellens JHM, Koomen G, and Schinkel AH (2002) Potent and specific inhibition of the breast cancer resistance protein multidrug transporter in vitro and in mouse intestine by a novel analogue of fumitremorgin C. *Mol Cancer Ther* 1: 417-425.

Boer J, Young-Sciame R, Lee F, Bowman KJ, Yang X, Shi JG, Nedza FM, Yeleswaram S, and Diamond S (2016) The role of UGT, CYP and Gut microbiota in the metabolism of epacadostat (EPA) in humans. *Drug Metab Dispos* 44: 1668-1674.

Borst P, Zelcer N, and van de Wetering K (2006) MRP2 and 3 in health and disease. *Cancer Lett* 234: 51-61.

Brouwer KL, Keppler D, Hoffmaster KA, Bow DA, Cheng Y, Lai Y, Palm JE, Stieger B, Evers R; International Transporter Consortium (2013) In vitro methods to support transporter evaluation in drug discovery and development. *Clin Pharmacol Ther* 94: 95-112.

de Waart DR, Vlaming ML, Kunne C, Schinkel AH, and Oude Elferink RP (2009) Complex pharmacokinetic behavior of ezetimibe depends on abcc2, abcc3, and abcg2. *Drug Metab Dispos* 37: 1698-1702.

Dobrinska MR (1989) Enterohepatic circulation of drugs. *J Clin Pharmacol* 29: 577-580.

EMA (2012) Guideline on the Investigation of Drug Interactions, European Medicines Agency, London, United Kingdom.

FDA (2012) Guidance for Industry: Drug Interaction Studies—Study Design, Data Analysis, Implications for Dosing, and Labeling Recommendations, U. S. Food and Drug Administration, Silver Spring, MD.

Giacomini KM, Huang SM, Tweedie DJ, Benet LZ, Brouwer KL, Chu X, Dahlin A, Evers R, Fischer V, Hillgren KM, Hoffmaster KA, Ishikawa T, Keppler D, Kim RB, Lee CA, Niemi M, Polli JW, Sugiyama Y, Swaan PW, Ware JA, Wright SH, Yee SW, Zamek-Gliszczynski MJ,

and Zhang L (2010) Membrane transporters in drug development. *Nat Rev Drug Disco* 9: 215-236.

Gui C, Miao Y, Thompson L, Wahlgren B, Mock M, Stieger B, and Hagenbuch B (2008) Effect of pregnane X receptor ligands on transport mediated by human OATP1B1 and OATP1B3. *Eur J Pharmacol* 584: 57-65.

Hirano M, Maeda K, Shitara Y, and Sugiyama Y (2006) Drug-drug interaction between pitavastatin and various drugs via OATP1B1. *Drug Metab Dispos* 34: 1229-1236.

Iusuf D, van de Steeg E, and Schinkel AH (2012) Hepatocyte hopping of OATP1B substrates contributes to efficient hepatic detoxification. *Clin Pharmacol Ther* 92: 559-562.

Köck K and Brouwer KL (2012) A perspective on efflux transport proteins in the liver. *Clin Pharmacol Ther* 92: 599-612.

Ni Z, Bikadi Z, Rosenberg MF, and Mao Q (2010) Structure and Function of the Human Breast Cancer Resistance Protein (BCRP/ABCG2). *Curr Drug Metab*11: 603-617.

Oswald S, König J, Lütjohann D, Giessmann T, Kroemer HK, Rimmbach C, Rosskopf D, Fromm MF, and Siegmund W (2008) Disposition of ezetimibe is influenced by polymorphisms of the hepatic uptake carrier OATP1B1. *Pharmacogenet Genomics* 18: 559-568.

Picard N, Yee SW, Woillard JB, Lebranchu Y, Le Meur Y, Giacomini KM, and Marquet P (2010) The role of organic anion-transporting polypeptides and their common genetic variants in mycophenolic acid pharmacokinetics. *Clin Pharmacol Ther* 87: 100-108.

Pou L, Brunet M, Cantarell C, Vidal E, Oppenheimer F, Monforte V, Vilardell J, Roman A, Martorell J, and Capdevila L (2001) Mycophenolic acid plasma concentrations: influence of comedication. *Ther Drug Monit* 23: 35-38.

Sampson KE, Brinker A, Pratt J, Venkatraman N, Xiao Y, Blasberg J, Steiner T, Bourner M, and Thompson DC (2015) Zinc finger nuclease-mediated gene knockout results in loss of

transport activity for P-glycoprotein, BCRP, and MRP2 in Caco-2 cells. *Drug Metab Dispos* 43: 199-207.

Shi JG, Chen X, Punwani NG, Williams WV, and Yeleswaram S (2016) Potential underprediction of warfarin drug interaction from conventional interaction studies and risk mitigation: a case study with epacadostat, an IDO1 inhibitor. *J Clin Pharmacol* 56: 1344-1354.

Shipkova M, Armstrong VW, Kuypers D, Perner F, Fabrizi V, Holzer H, Wieland E, and Oellerich M (2001) Effect of cyclosporine withdrawal on mycophenolic acid pharmacokinetics in kidney transplant recipients with deteriorating renal function: preliminary report. *Ther Drug Monit* 23: 717-721.

Vasilyeva A, Durmus S, Li L, Wagenaar E, Hu S, Gibson AA, Panetta JC, Mani S, Sparreboom A, Baker SD, and Schinkel AH (2015) Hepatocellular Shuttling and Recirculation of Sorafenib-Glucuronide Is Dependent on Abcc2, Abcc3, and Oatp1a/1b. *Cancer Res* 75: 2729-2736.

Zamek-Gliszczynski MJ, Chu X, Polli JW, Paine MF, and Galetin A (2014) Understanding the transport properties of metabolites: case studies and considerations for drug development. *Drug Metab Dispos* 42: 650-664.

Zamek-Gliszczynski MJ, Nezasa K, Tian X, Bridges AS, Lee K, Belinsky MG, Kruh GD, and Brouwer KL (2006) Evaluation of the role of multidrug resistance-associated protein (Mrp) 3 and Mrp4 in hepatic basolateral excretion of sulfate and glucuronide metabolites of acetaminophen, 4-methylumbelliferone, and harmol in Abcc3-/- and Abcc4-/- mice. *J Pharmacol Exp Ther* 319: 1485-1491.

Zhang Y, Han YH, Putluru SP, Matta MK, Kole P, Mandlekar S, Furlong MT, Liu T, Iyer RA, Marathe P, Yang Z, Lai Y, and Rodrigues AD (2016) Diclofenac and its acyl glucuronide: determination of in vivo exposure in human subjects and characterization as human drug transporter substrates in vitro. *Drug Metab Dispos* 44: 320-328.

Footnotes

The current affiliation of Jack G. Shi is Ultragenyx Pharmaceutical Company.

Financial disclosure: All authors are/were employees and stock holders of Incyte Corporation.

DMD Fast Forward. Published on March 10, 2017 as DOI: 10.1124/dmd.116.074609
This article has not been copyedited and formatted. The final version may differ from this version.

Figure Legends

Figure 1. Chemical structures of EPAC, M9, M11, and M12 (Boer et al., 2016)**.** (All of the metabolites are pharmacologically inactive).

Figure 2. Plasma concentration-time profiles of EPAC in individual healthy subjects following 5 days of oral administration of 300 mg EPAC twice a day.

Figure 3. Transport of EPAC and its metabolites by human P-gp in Caco-2 cell monolayers and by human BCRP in MDCKII-BCRP cell monolayers or membrane vesicles containing BCRP. (A to D) Caco-2 cell monolayers. White bar represents the efflux ratio in the presence of vehicle (DMSO). Black bar represents the efflux ratio in the presence of P-gp inhibitor cyclosporine A (5 μM). Digoxin (5 μM) was included as the positive control substrate for P-gp. (E, G, and H) MDCKII-BCRP cell monolayers**.** White bar represents the efflux ratio in control cell monolayers. Black bar represents the efflux ratio in MDCKII-BCRP cell monolayers. Prazosin (1 μM) and Ko143 (3 μM) were included as the positive control substrate and inhibitor for BCRP, respectively. (F) Membrane vesicles containing BCRP. White bar represents the uptake rate in the presence of ATP. Black bar represents the uptake rate in the presence of AMP. Shaded bar represents the uptake rate in the presence of ATP and a BCRP inhibitor Ko143 (1 μM). Estrone 3-sulfate (1 μM) was included as the positive control substrate for BCRP. Results are shown as the mean ± S.D. (n = 3).

Figure 4. Transport of EPAC in P-gp/MRP2 double knockout and BCRP/MRP2 double knockout Caco-2 cell lines. Black bar represents the efflux ratio in the presence of a BCRP inhibitor Ko143 (3 μM) (A and B) or a P-gp inhibitor verapamil (100 μM) (C and D). White bar represents the efflux ratio in the absence of an inhibitor. Estrone 3-sulfate (10 μM) and digoxin

DMD Fast Forward. Published on March 10, 2017 as DOI: 10.1124/dmd.116.074609
This article has not been copyedited and formatted. The final version may differ from this version.

(10 μM) were included as the positive control substrate for BCRP and P-gp, respectively. Results are shown as the mean ± S.D. (n = 3).

Figure 5. Time-dependent uptake of EPAC and its metabolites into human OATP1B1 and OATP1B3 transfected CHO cells. Black square represents the uptake in the transporter-transfected cells. White square represents the uptake in the control cells. The concentrations of EPAC, M9, M11, and M12 were 10, 10, 5, and 5 μM, respectively. Results are shown as the mean ± S.D. (n = 3).

Figure 6. Uptake of EPAC and M9 into human OATP1B1 and OATP1B3 transfected CHO cells in the absence or presence of cerivastatin (an inhibitor of OATP1B1 and OATP1B3). The uptake of EPAC (5 μM), M9 (10 μM), and control substrate pitavastatin (0.5 μM) were conducted in the transporter-transfected and control CHO cells in the absence or presence of an inhibitor (cerivastatin). The incubation time with EPAC, M9, or pitavastatin was 1, 5, and 1 min, respectively. White bar represents the uptake rate in the presence of vehicle (DMSO). Black bar represents the uptake rate in the presence of 100 μM cerivastatin. CRS denotes cerivastatin. Results are shown as the mean ± S.D. (n = 3). Significance was determined by a Student *t* test when an inhibitor treatment was compared to DMSO control (**P* < 0.05, ***P* < 0.01, ****P* < 0.001).

Figure 7. Transport of M9 by human MRP2 and MRP3 in membrane vesicles containing human MRP2 or MRP3. Uptake of M9 (3 and 30 μM) and control substrate estradiol 17-β-D-glucuronide (50 μM) was conducted in the membrane vesicles in the presence or absence of inhibitors, and with or without ATP. The incubation time was 8 min. White bar represents the uptake rate in the presence of ATP. Black bar represents the uptake rate in the presence of AMP. Shaded bar represents the uptake rate in the presence of a MRP2 inhibitor (400 μM

DMD Fast Forward. Published on March 10, 2017 as DOI: 10.1124/dmd.116.074609
This article has not been copyedited and formatted. The final version may differ from this version.

benzbromarone) with ATP or a MRP3 inhibitor (1 mM sulfasalazine) with ATP. Results are shown as the mean ± S.D. (n = 3).

Figure 8. Illustration of the hypothesized mechanisms of disposition of EPAC and its metabolites in humans. After oral administration of EPAC, a fraction of EPAC (green particles) in the gut lumen is metabolized to form M11 (orange particles) via gut microflora. Due to their moderate membrane permeability, both EPAC and M11 enter enterocytes and subsequently cross the basolateral membrane of enterocytes to reach the portal vein by passive diffusion. A fraction of EPAC inside of enterocytes may be excreted back to the gut lumen by both BCRP and P-gp. In the liver, EPAC and M11 in the blood can passively diffuse into hepatocytes where EPAC is metabolized by UGT1A9 to form EPAC glucuronide (M9) (blue particles) and M11 is further metabolized by CYP3A4 primarily to form M12 (red particles). The portion of EPAC molecules which are not metabolized can diffuse passively or be excreted by BCRP and P-gp in the canalicular membrane into the bile. M9 molecules formed in hepatocytes are either excreted into the bile via MRP2 and BCRP or excreted to the blood via MRP3 in the sinusoidal membrane. Once in the blood, M9 can be taken up into the downstream hepatocytes via OATP1B1 and OATP1B3, and subsequently be excreted into the bile by MRP2 and BCRP. This process of excretion-reuptake is referred as “hepatocyte hopping”, which can prevent the saturation of active biliary excretion in the upstream hepatocytes, and facilitate efficient biliary elimination and flexible detoxification of endogenous compounds and drug conjugates in the liver. Both EPAC and M9 in the bile move to the intestine lumen where M9 can be converted back to parent EPAC by gut microflora. The regenerated EPAC may be reabsorbed in the gut, which is the EHC phenomenon observed in the human pharmacokinetics of EPAC.

DMD Fast Forward. Published on March 10, 2017 as DOI: 10.1124/dmd.116.074609
This article has not been copyedited and formatted. The final version may differ from this version.

Tables

Table 1. Summary of the in vitro models used in the present article

In vitro model	Transporter	Assay	Compound	Purpose
Parental Caco-2 monolayers	P-gp	Transcellular transport	EPAC, M9, M11, M12	Substrate and inhibition
Knock-out Caco-2 monolayers	P-gp BCRP	Transcellular transport	EPAC	Substrate
Transfectant MDCKII monolayers	BCRP	Transcellular transport	EPAC, M9, M11, M12	Substrate and inhibition
Transfectant CHO cells	OATP1B1 OATP1B3	Uptake	EPAC, M9, M11, M12	Substrate and inhibition
Transfectant CHO cells	OAT1 OCT2	Uptake	EPAC, M9, M11, M12	Inhibition
Transfectant HEK cells	OAT3	Uptake	EPAC, M9, M11, M12	Inhibition
Membrane vesicles	MRP2, MRP3, BCRP	Uptake	M9	Substrate

DMD Fast Forward. Published on March 10, 2017 as DOI: 10.1124/dmd.116.074609
This article has not been copyedited and formatted. The final version may differ from this version.

Table 2. Physicochemical properties and permeability of EPAC, M9, M11, and M12.

Compound	MW (g/mol)	logP[a]	PSA[a]	Caco-2 P_{app} (10^{-6} cm/s)
EPAC	438.2	2.17	168	4.0
M9	614.4	-2.1	264	< 0.1
M11	422.2	0.61	159	3.2
M12	300.1	1.9	101	9.3

[a] Calculated by ADMET Predictor software (Simulations Plus, Lancaster, CA).

DMD Fast Forward. Published on March 10, 2017 as DOI: 10.1124/dmd.116.074609
This article has not been copyedited and formatted. The final version may differ from this version.

Table 3. In vitro evaluation of EPAC and its metabolites as an inhibitor of efflux transporters P-gp, BCRP, and uptake transporters OATP1B1, OATP1B3, OAT1, OAT3, and OCT2.

Compound	IC_{50} (μM)						
	P-gp	BCRP	OATP1B1	OATP1B3	OAT1	OAT3	OCT2
EPAC	>500	N/I	59	51	>300	21	203
M9	N/I	N/I	262	27	N/I	>300	N/I
M11	N/I	>300	68	19	N/I	14	23
M12	N/I	32	49	228	8.6	21	21

N/I = No inhibition was observed over the range of the concentrations tested.

DMD Fast Forward. Published on March 10, 2017 as DOI: 10.1124/dmd.116.074609
This article has not been copyedited and formatted. The final version may differ from this version.

Table 4. In vitro evaluation of EPAC and its metabolites as a potential perpetrator for P-gp- or BCRP-mediated drug-drug interactions.

Compound	I_1 (μM)	I_2 (μM)	P-gp			BCRP		
			IC_{50} (μM)	I_1/ IC_{50}	I_2/ IC_{50}	IC_{50} (μM)	I_1/ IC_{50}	I_2/ IC_{50}
EPAC	1.57	2740	>500	<0.004	<5.5	N/I	N/A	N/A
M9	10.2	unknown	N/I	N/A	N/A	N/I	N/A	N/A
M11	2.10	unknown	N/I	N/A	N/A	>300	<0.007	N/A
M12	2.10	unknown	N/I	N/A	N/A	32	0.066	N/A

N/I = No inhibition was observed over the range of the concentrations tested.

N/A = Not applicable.

I_1 = Mean steady-state total C_{max} following 300 mg BID dose

I_2 = 300 mg (0.685 mmol) dose divided by 250 ml

DMD Fast Forward. Published on March 10, 2017 as DOI: 10.1124/dmd.116.074609
This article has not been copyedited and formatted. The final version may differ from this version.

Table 5. In vitro evaluation of EPAC and its metabolites as a potential perpetrator for OATP1B1- or OATP1B3-mediated drug-drug interactions.

Compound	Total C_{max} (μM)	OATP1B1			OATP1B3		
		IC_{50} (μM)	C_{max}/IC_{50}	R value	IC_{50} (μM)	C_{max}/IC_{50}	R value
EPAC	2.5	59	0.042	1.008	51	0.049	1.009
M9	10.2	262	0.039	1.007[a]	27	0.38	1.072[a]
M11	2.1	68	0.031	1.004[a]	19	0.11	1.014[a]
M12	2.1	49	0.043	1.002[a]	228	0.009	1.000[a]

[a] These values were calculated by using the maximum total plasma concentrations in the clinical studies instead of using $I_{in,max}$ due to lack of certain parameters for the estimation of the $I_{in,max}$ value. Refer to the "Materials and Methods" section for the details of the R value calculation.

DMD Fast Forward. Published on March 10, 2017 as DOI: 10.1124/dmd.116.074609
This article has not been copyedited and formatted. The final version may differ from this version.

Table 6. In vitro evaluation of EPAC and its metabolites as a potential perpetrator for OAT1- , OAT3 or OCT2-mediated drug-drug interactions.

Compound	Free C_{max} (μM)	OAT1		OAT3		OCT2	
		IC_{50} (μM)	C_{max}/IC_{50}	IC_{50} (μM)	C_{max}/IC_{50}	IC_{50} (μM)	C_{max}/IC_{50}
EPAC	0.049	>300	<0.0002	21	0.002	203	0.0002
M9	1.95	N/I	N/A	>300	<0.007	N/I	N/A
M11	0.263	N/I	N/A	14	0.019	23	0.011
M12	0.080	8.6	0.009	21	0.004	21	0.004

N/I = No inhibition was observed over the range of the concentrations tested.

N/A = Not applicable.

DMD Fast Forward. Published on March 10, 2017 as DOI: 10.1124/dmd.116.074609
This article has not been copyedited and formatted. The final version may differ from this version.

Figure 1

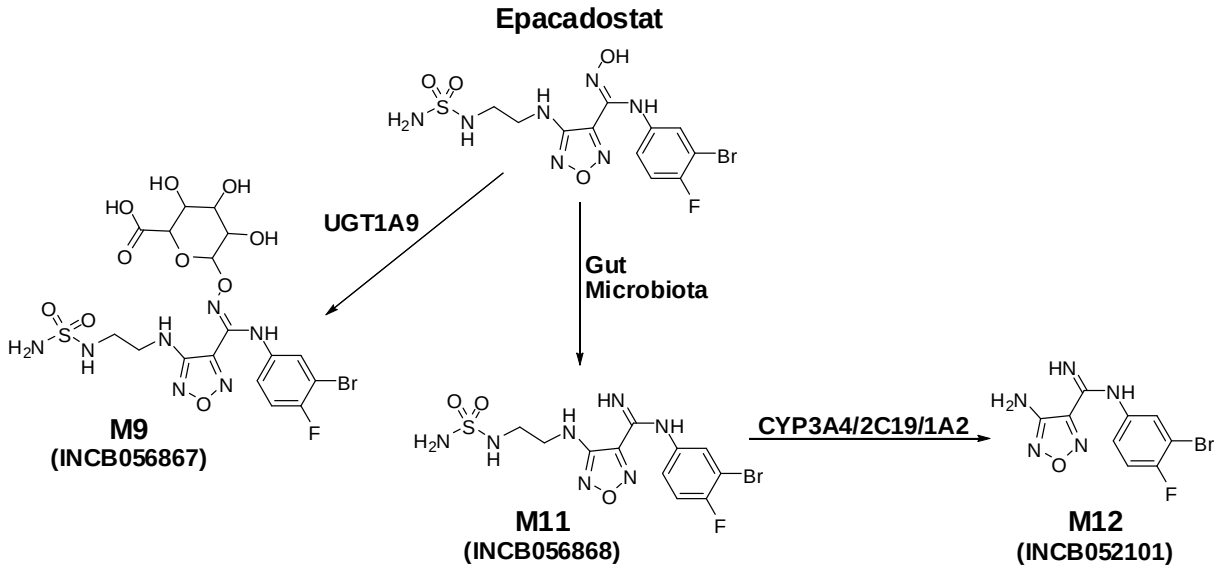

DMD Fast Forward. Published on March 10, 2017 as DOI: 10.1124/dmd.116.074609
This article has not been copyedited and formatted. The final version may differ from this version.

Figure 2

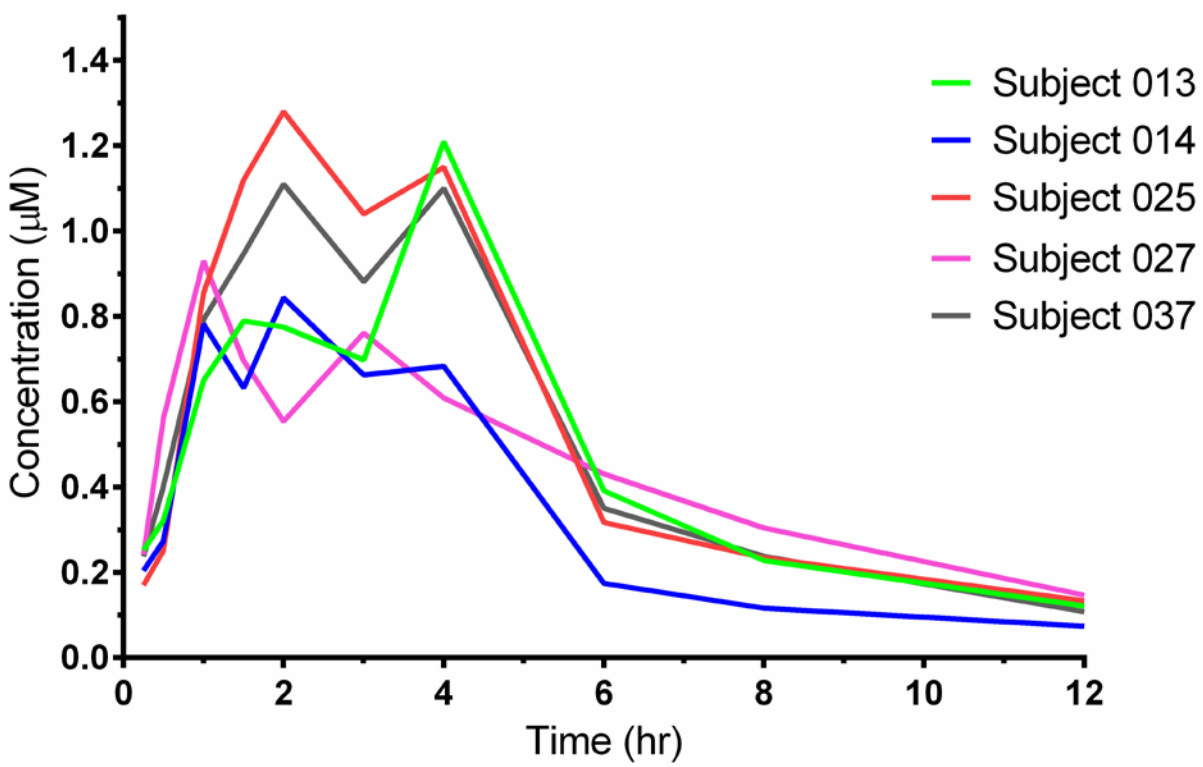

DMD Fast Forward. Published on March 10, 2017 as DOI: 10.1124/dmd.116.074609
This article has not been copyedited and formatted. The final version may differ from this version.

Figure 3

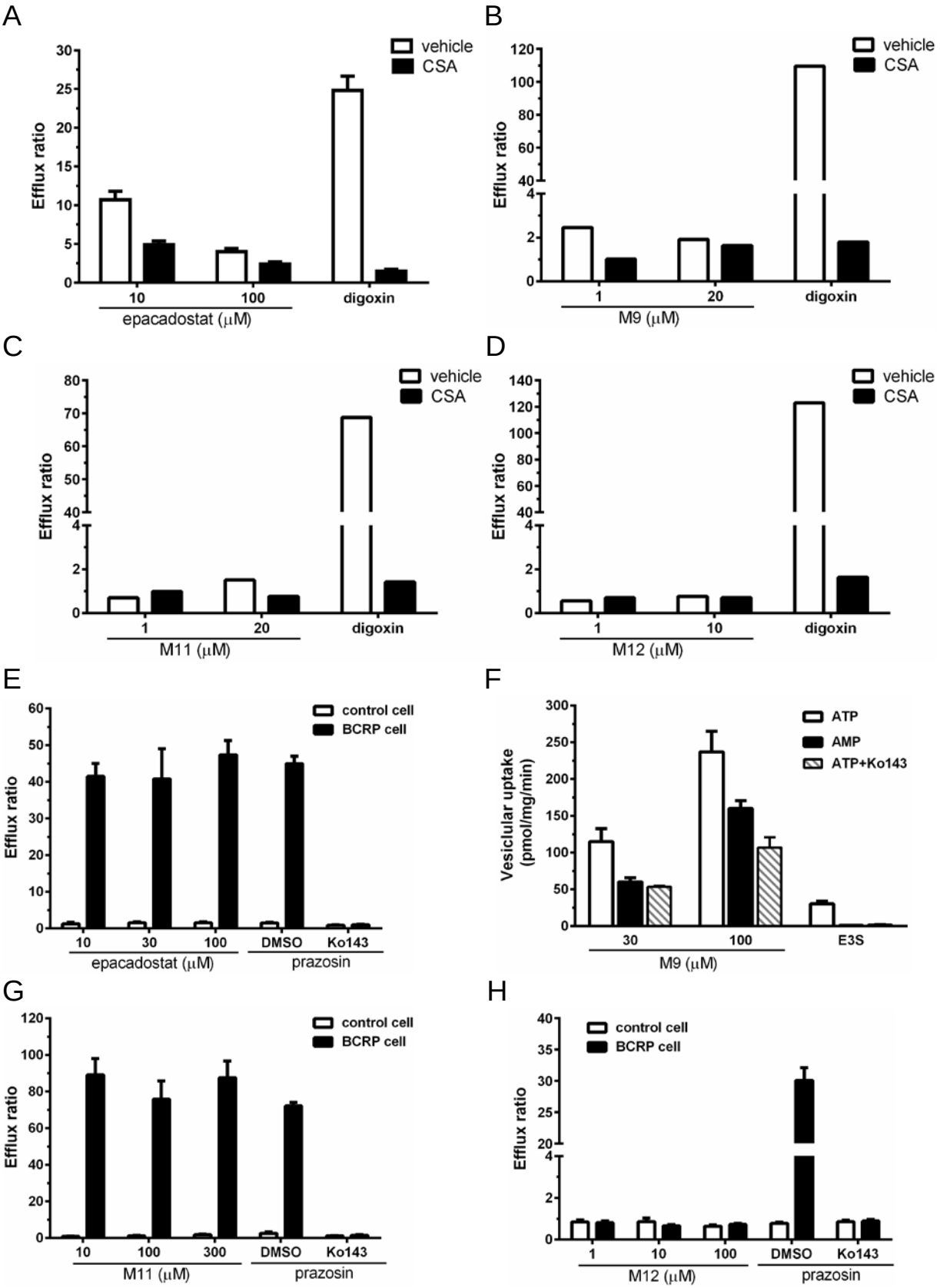

DMD Fast Forward. Published on March 10, 2017 as DOI: 10.1124/dmd.116.074609
This article has not been copyedited and formatted. The final version may differ from this version.

Figure 4

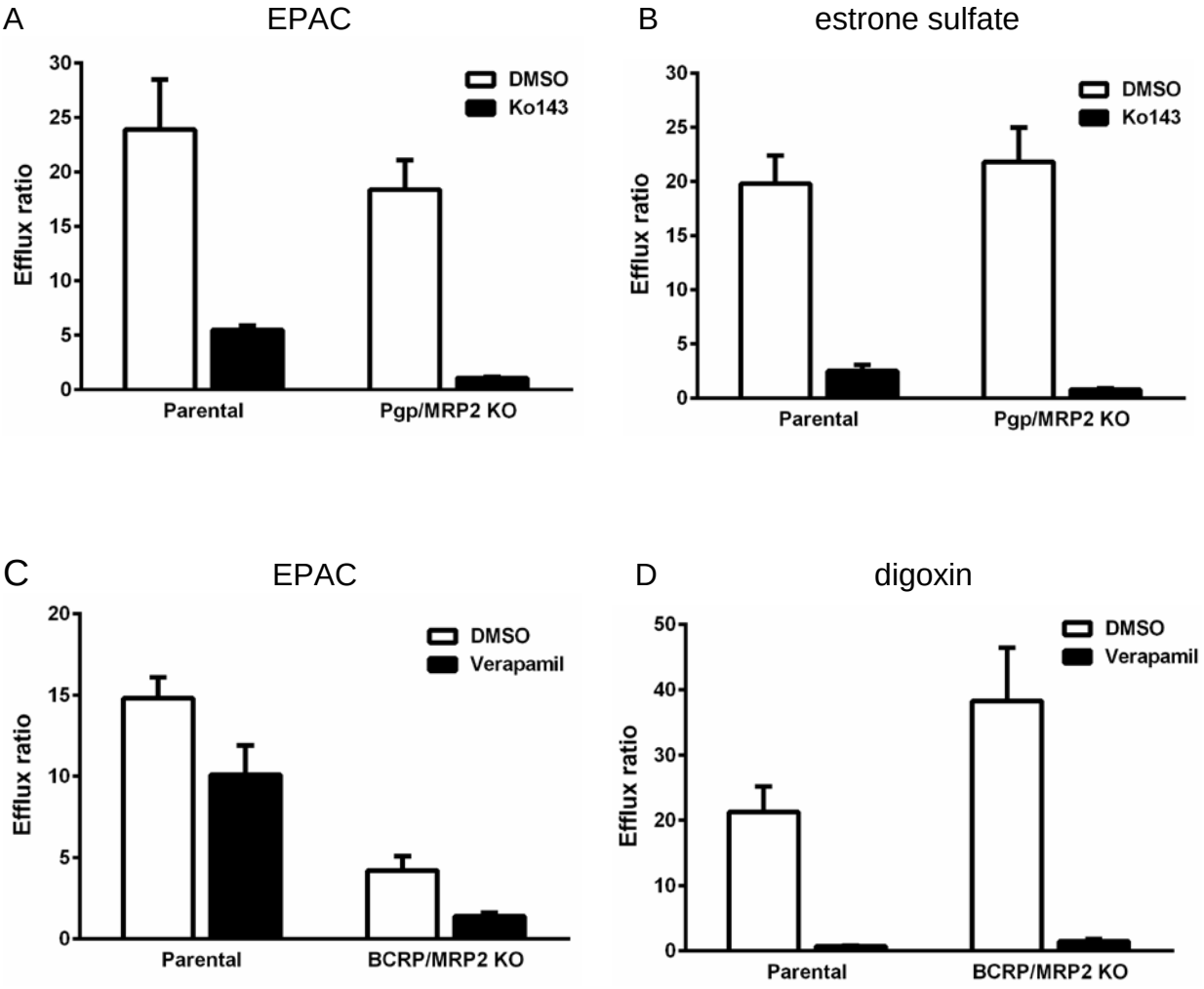

DMD Fast Forward. Published on March 10, 2017 as DOI: 10.1124/dmd.116.074609
This article has not been copyedited and formatted. The final version may differ from this version.

Figure 5

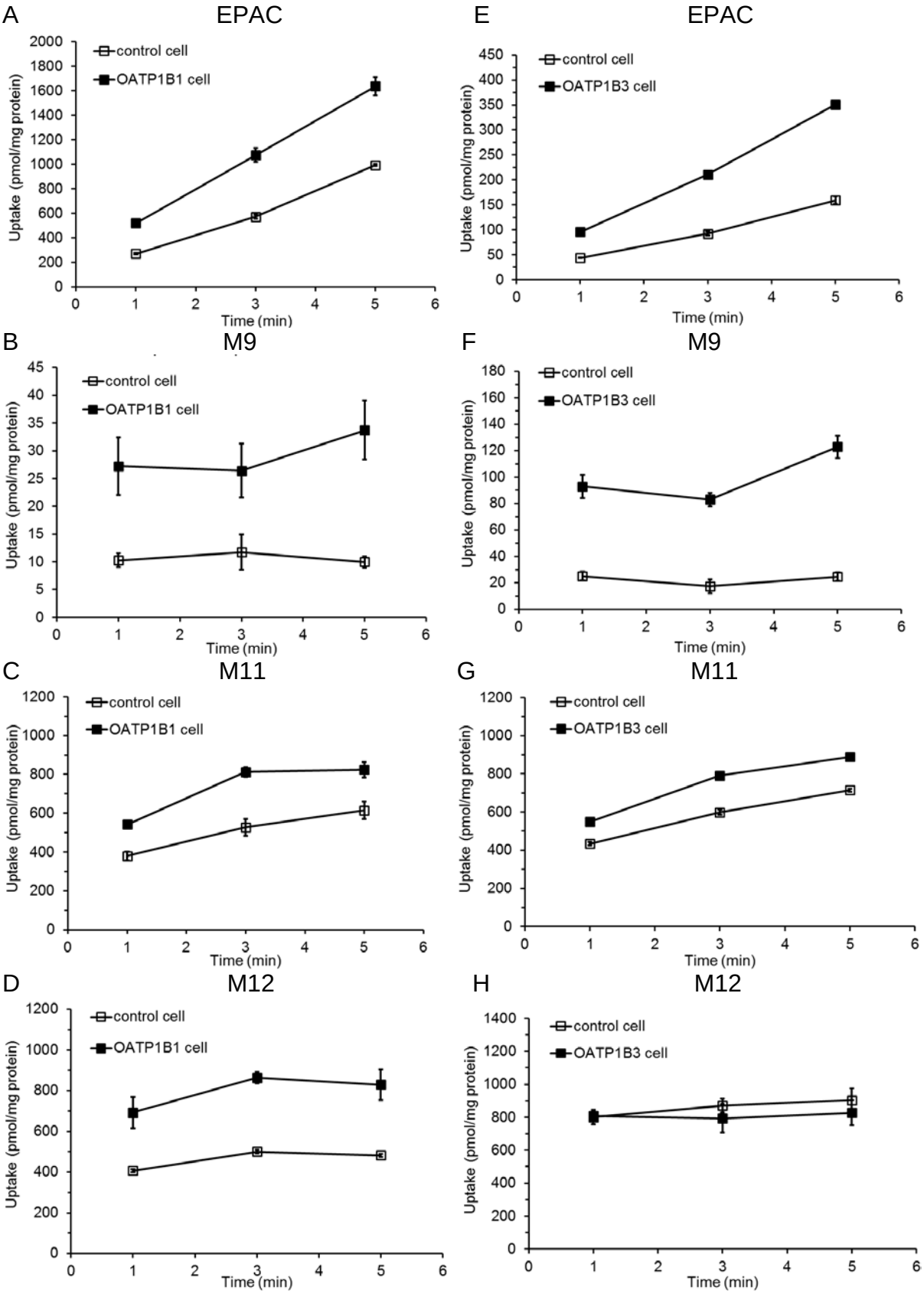

DMD Fast Forward. Published on March 10, 2017 as DOI: 10.1124/dmd.116.074609
This article has not been copyedited and formatted. The final version may differ from this version.

Figure 6

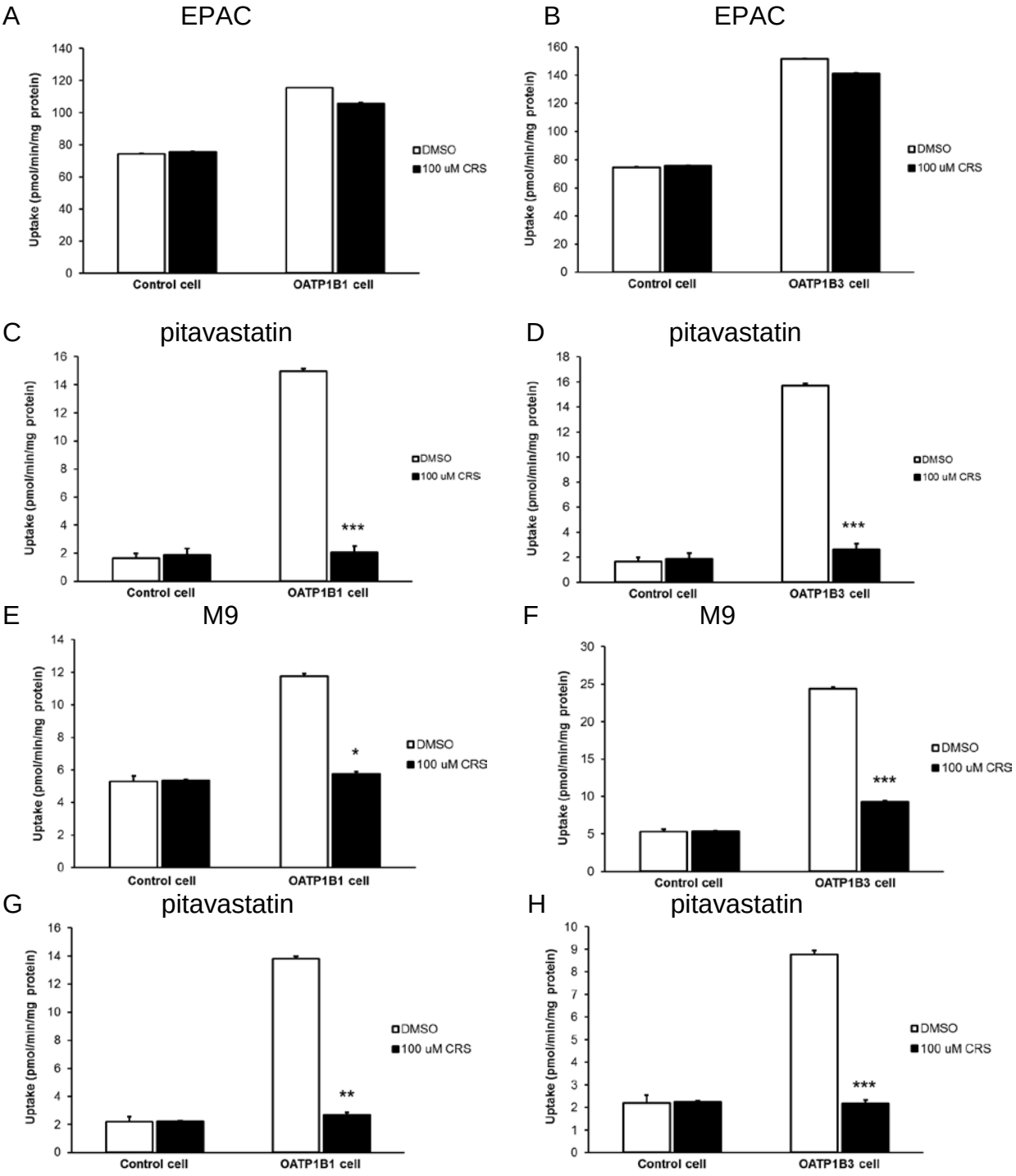

DMD Fast Forward. Published on March 10, 2017 as DOI: 10.1124/dmd.116.074609
This article has not been copyedited and formatted. The final version may differ from this version.

Figure 7

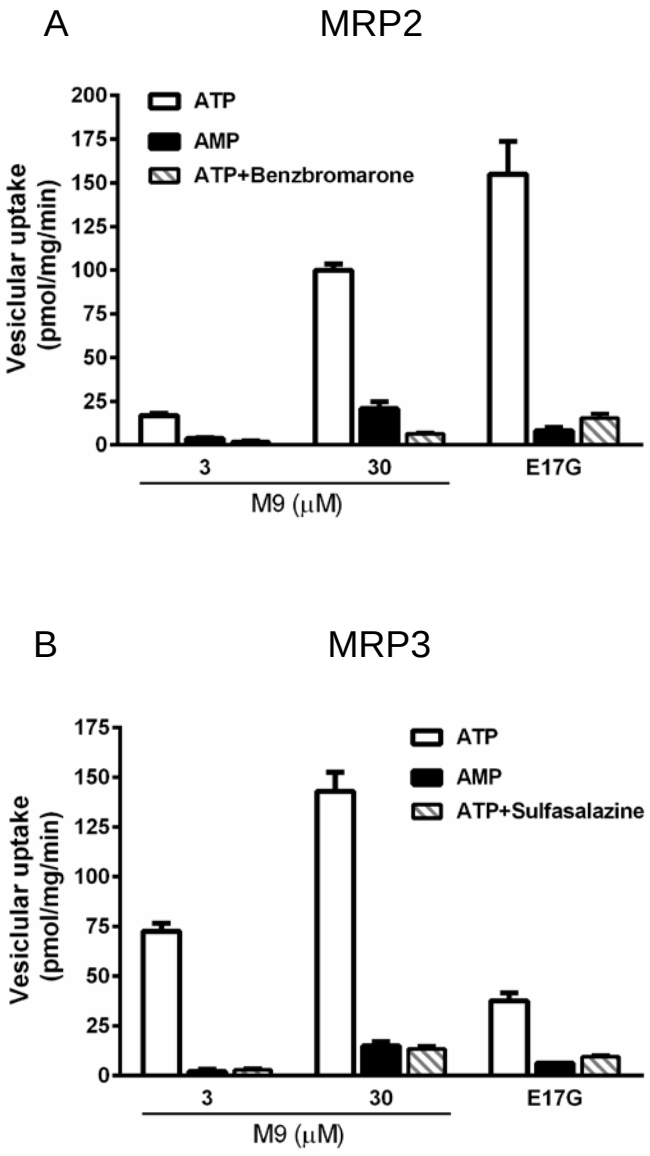

DMD Fast Forward. Published on March 10, 2017 as DOI: 10.1124/dmd.116.074609
This article has not been copyedited and formatted. The final version may differ from this version.

Figure 8